Coherent Communication Over Multi Mode Fibers for Intra-Datacenter Ultra-High Speed Links

(Article begins on next page)

12 June 2023

Coherent Communication Over Multi Mode Fibers for Intra-Datacenter Ultra-High Speed Links

Giuseppe Rizzelli , Pablo Torres Ferrera , Fabrizio Forghieri, *Senior Member, IEEE*, Antonello Nespola, Andrea Carena , *Senior Member, IEEE*, and Roberto Gaudino , *Senior Member, IEEE*

Abstract—Multimode fibers (MMFs) links using vertical cavity surface-emitting lasers (VCSELs) are still the solution of choice for today's data center shorter distances thanks to their low cost and robustness. Currently, the market is moving towards 400G-capable systems using multiple lanes at 50 Gbps per lane, based on intensity modulation (IM) and direct detection (DD). A technology switch will probably be required to overcome the 100 Gbps per lane limit that will likely be the bottleneck of future IM-DD MMF-based links. In this manuscript we propose an intra-data center system based on coherent detection and MMF, analyzing experimentally and analytically the performance of polarization multiplexed coherent communication. We show that the advantages enabled by the coherent technology can be fully exploited in an MMF-based link when central launch is ensured. In particular, we study in detail the effect of lateral offsets introduced by the connectors at the interface between two MMF facets, in terms of net optical loss and signal-to-noise ratio (SNR) degradation. A statistical analysis is performed analytically exploiting a large database of OM3 and OM4 fibers modal delays and results are presented for various combinations of fiber length, type and number of MMF-to-MMF connections along the link. We show quantitative results on the maximum acceptable lateral offsets in the MMF connectors, highlighting that in practical conditions average offsets of up to 3 μm can be tolerable.

Index Terms—Coherent detection, multi mode fibers, intra data-center interconnection.

I. Introduction

IN INTRA-DATA center (IDC) interconnects, multimode fibers are largely deployed for distances up to 300 m since they enable using VCSEL-based transceivers at 850 nm, which have significantly lower costs than all other short reach options. However, VCSEL+MMF transmission, even with newer OM4

Giuseppe Rizzelli is with LINKS Foundation, 10138, TO Torino, Italy, and also with the Department of Electronics and Telecommunications, Politecnico di Torino, 10129, TO Torino, Italy (e-mail: giuseppe.rizzelli@polito.it).

Pablo Torres Ferrera, Andrea Carena, and Roberto Gaudino are with the Department of Electronics and Telecommunications, Politecnico di Torino, 10129, TO Torino, Italy (e-mail: pablo.torres@polito.it; andrea.carena@polito.it; roberto.gaudino@polito.it).

Fabrizio Forghieri is with the CISCO Photonics Italy, 20871, MB Vimercate, Italy (e-mail: fforghie@cisco.com).

Antonello Nespola is with the LINKS Foundation, 10138, TO Torino, Italy (e-mail: antonino.nespola@linksfoundation.com).

Color versions of one or more figures in this article are available at https://doi.org/10.1109/JLT.2022.3174422.

Digital Object Identifier 10.1109/JLT.2022.3174422

and OM5 grade fibers, have well-known maximum capacity limits due to multimodal dispersion [1], that make today transmission at more than 50 Gbit/s per wavelength over 300 m a difficult task. In fact, to date, transmission speed up to 28 Gbps per lane over 70 m and 100 m using OM3 and OM4 fibers is obtained by commercial solutions defined in Ethernet 100GBASE-SR4 and Fiber Channel (FC) 32G-FC standards, that rely on Intensity Modulation and Direct Detection (IM-DD) using 25G-class devices, on-off keying (OOK) modulation and legacy fibers. Alternatives such as 400GBASE-SR8 and 400GBASE-SR4.2 enable 50 Gbps/λ with PAM-4 modulation over 100 m of OM4 or 70 m of OM3 fiber. Moreover, recent works have demonstrated extended reach up to 250 m using short wavelength division multiplexing (SWDM) at 25 Gbps/λ and 4 wavelengths (850, 880, 910, and 940 nm) on newly developed OM5 or wideband OM4 fibers, thus achieving 100 G transmission at the cost of a completely renovated MMF fiber plant [2].

Capacity upgrade is even more difficult on older multimode fibers (OM2 and OM3), that are anyway still very common today in IDC for very high speed short reach optical interconnects. It would be in principle very interesting to upgrade achievable bit rates without having to change the installed MMF fibers. In fact, although the percentage of MMF optical lines is decreasing compared to SMF solutions, they are still being installed in numbers of more than 20 million per year [3] and represent 50% of the total for rates up to 100 G and over 30% for rates up to 400G [4]. The volumes of installed MMF ports in IDC is thus still huge, and it justifies research work towards enabling even higher bit rates. In two previous preliminary conference papers ([5] and [6]), we have thus investigated the possibility of using commercial coherent transceivers over MMF fibers (indicating the setup as "coherent-over-MMF" or Coh-MMF) showing, somehow unexpectedly, excellent performances up to 400 Gbps over 300 m OM3 multimode fibers. In the present paper, we largely expand our previous work from both a theoretical point of view, analyzing by a detailed numerical simulator the performance of Coh-MMF systems, and from an experimental point of view, showing a different set of measurements compared to those presented in [6].

Several previous papers have already discussed coherent detection for the future short reach IDC ecosystem when using standard single mode fibers (SMF), as an interesting option for transitioning from today IM-DD commercial solutions running at up to 100 G per wavelength to future coherent 400 G or even 800 G per wavelength, mostly given the remarkable

improvement in sensitivity that coherent solutions can provide even in optically un-amplified solutions [7]. However, it is well known that all coherent transceivers are "natively" coupled to SMF fibers. For an usage extension to MMF, we thus proposed an SMF-MMF-SMF configuration, i.e. a solution in which standard SMF coherent transceivers are directly coupled to the MMF link. As already demonstrated [8]–[11], an SMF-MMF-SMF transmission system works as a "quasi single-mode" one provided that the involved SMF and MMF fibers are centrally aligned. In this case, most of the optical power launched in the transmitter (TX) SMF couples to the fundamental (LP_{01}) mode of the MMF and, at its output, to the receiver SMF. [9]–[11] already demonstrated coherent transmission over MMF up to 100 Gbps, showing that the "quasi-single mode operation" works well, even at extremely long distances such as the 200 km and 635 km reach shown respectively in [9] and [11], as long as the central launch conditions are preserved. Overall, a centrally aligned SMF-MMF-SMF system can have extra losses well below 2 dB.

In a practical IDC environment, the MMF section itself can be made of several pieces of MMF interconnected through standard-grade connectors inside patch panels. At the transition between an SMF and an MMF, or at the interface between two MMFs, all the propagating modes couple to each other in a random way affected by the geometrical properties of the fiber facets. Moreover, slight misalignment between the fibers core can contribute to modes mixing unpredictably before coupling back to the fundamental LP_{01} mode of the last SMF fiber before the receiver (RX).

In this paper, we thus study the propagation of the modes in the SMF-MMF-SMF system, focusing mostly on estimating the maximum acceptable lateral offsets in MMF connectors. We show that in realistic datacenter conditions up to 3 μm average values of lateral offset can be tolerated in practical conditions. We calculate the coupling coefficients among the modes using the analytical model presented in [12] and we show that mode coupling changes the way the modal dispersion impact the propagating signal, because of a different excitation pattern. Thus, the overall transfer function changes due to the birefringence of the fiber and to the offset introduced by the connectors at the interface between two fibers. By using the model presented in [13], properly modified to include the effect of the birefringence experienced by each mode during transmission of a polarization multiplexed (PM) signal, we generate the transfer function of the system and then use it to compute the performance of a coherent detection-based transmission system. The system performance are finally obtained through another analytical model [14] that assumes ideal equalization with an infinite number of taps, modified to take into account transmission on two polarizations.

Our results are of practical interest for IDC situations having a large installed MMF infrastructure, which could be upgraded to much higher bit rates by changing only the transceivers (from IM-DD to Coh-MMF) without substituting the MMF plant. Obviously, the cost saving due to MMF re-use is traded-off by the significantly higher cost of coherent transceivers, but this techno-economic discussion is outside the scope of our paper. We just point out that coherent transceiver cost and power consumption is currently being tackled by the Optical Internetworking Forum (OIF) who created the 400G-ZR standard, defining specifications for low-cost pluggable coherent modules [15]. Future technological developments may in the short term bring cost, power consumption and size of 400 G coherent transceivers down to values comparable to their current IM-DD counterparts [16].

The remainder of this manuscript is organized as follows: in Section II we introduce the full analytical model for the computation of the mode coupling coefficients, the overall system transfer function and of the RX equalizer performance in an SMF-MMF-SMF-based coherent system. In Section III we present the results of the Monte-Carlo-based statistical analysis of the transmission performance of a 200 Gbit/s (25 GBaud) PM-16QAM Coh-MMF system varying fiber characteristics such as modal delay, birefringence, length and type (OM3 or OM4). We also consider a variable number of connectors along the optical fiber path, each introducing a variable offset distributed as a Rayleigh random variable with variable mean [17], [18]. In Section IV we show the experimental results achieved with a real-time card running a 200 Gbit/s PM-16QAM modulated coherent communication over 296 m of OM3 MMF. Experiments have been performed for different offsets introduced by properly splicing two sections of MMF. Lastly, in Section V we discuss the implications of the presented results and draw some conclusions.

II. A SIMULATIVE MODEL FOR FIELD-LEVEL PROPAGATION IN SMF-MMF-SMF LINKS

The typical approach for IM-DD MMF links modeling is the one used by the Telecommunications Industry Association (TIA) for multimode fiber standards definition [20], where mode propagation inside an MMF and the coupling of modes at the connection between MMFs are numerically addressed considering the power distribution per *mode group* and their differential modal delay. In contrast, in SMF-MMF-SMF systems it is necessary to develop a numerical model that considers each *individual mode* propagating in the fibers. The final goal of this section is to compute the resulting frequency transfer function between the LP_{01} launched in the TX SMF to the LP_{01} in the RX SMF (after passing through the link MMF). We anticipate that, since we are interested in polarization multiplexed quadrature-amplitude modulation (PM-QAM) transmission, we will have to consider, besides modal dispersion, also fiber birefringence and polarization effects so that our final goal is to find the frequency-resolved [2 × 2] Jones matrix of the full SMF-MMF-SMF link.

A. SMF-MMF-SMF System Without MMF Connectors

In this subsection we introduce a simplified analysis of our Coh-MMF system that will allow to grasp a first insight of the propagation behaviour of an SMF-MMF-SMF link. Here we intentionally neglect the problem of lateral offsets in connectors along the MMF fiber, an issue that will be treated in detail in the next Subsection. We consider that the signal generated by the coherent transmitter propagates over a very short SMF fiber
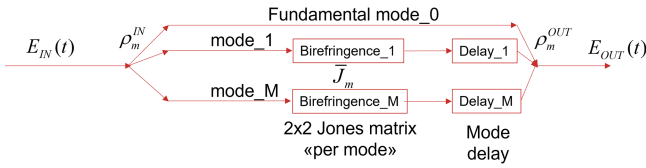
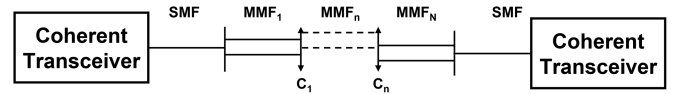Fig. 1. Scheme representing SMF-MMF-SMF propagation model (for a single MMF span) as in (1).

Fig. 2. Setup of the Coh-MMF transmission system with SMF-MMF-SMF configuration. MMF: Multimode Fiber; SMF: Single Mode Fiber; C: Connector.

pigtail (i.e. the one that is typically present inside commercial coherent transceivers), then it is coupled to the MMF link, where higher order modes above the LP_{01} fundamental mode are able to propagate as well, and finally is coupled back into the SMF pigtail inside the coherent receiver. We will show that the resulting end-to-end frequency transfer function seen by the coherent transceiver depends on i) the coupling between the modes at each fiber transition, ii) the different delays between MMF modes and iii) the birefringence seen by each mode in the MMF.

To take into account the differential modal delays in the MMF, we use the large database of measured modal delays presented in [21]. Moreover, we assume that, to a first order approximation, the modes belonging to the same mode group strongly couple to each other and have the same modal delay, while modes belonging to different mode groups only marginally couple, a reasonable assumption as shown in [22] unless the fiber is strongly bent or twisted. Finally, we also need to consider that each mode is actually a pair of orthogonal polarization modes that propagate with their own random birefringence, as we pictorially represent in Fig. 1. Due to all these propagation effects, we can then express the relation between the $\vec{E}_{\mathrm{in}}$ field of the LP_{01} of the first SMF fiber (i.e. the signal generated by the coherent TX) and the $\vec{E}_{\mathrm{out}}$ field at the output of the last SMF section (i.e. the signal received by the coherent RX) as follows:

$$\vec{E}_{\mathrm{out}}(t) = \sum_{m=0}^{M-1} \rho_m^{\mathrm{in}} \boldsymbol{J}_m \cdot \vec{E}_{\mathrm{in}}(t - \tau_m) \rho_m^{\mathrm{out}} \qquad (1)$$

where M is the total number of modes of the MMF, m is the index of the mth mode of the MMF, ρ_m^{in} is the coupling coefficient between the LP_{01} mode of the input SMF and the mth mode of the MMF, ρ_m^{out} is the coupling coefficient between the mth mode of the MMF and the LP_{01} of the output SMF, $\boldsymbol{J}$ is the unitary random Jones matrix that takes into account "per mode" fiber birefringence and τ_m is the modal delay of the mth mode inside the MMF. Without loss of generality, and only to simplify the equations, we referred all delays and birefringence to those of the fundamental LP_{01} mode, therefore $\tau_0 = 0$. For all the coupling coefficients, we use the theory developed in [12], which allows to analytically obtain the $\rho_{m,k}$ coupling coefficients for generic lateral offsets in the fiber connections, under the assumption of infinitely parabolic refractive index profile in the MMF, by solving the overlap integral between the transverse field profile of the mth mode in the input fiber and the kth mode in the output fiber. In the following derivation, we consider a graded-index 50 μm core MMF.

(1) and its graphical representation in Fig. 1 highlight the key principle of operation of the proposed system, showing that if the ρ_m^{in} coefficients are all sufficiently smaller (in modulus) than ρ_0^{in} and ρ_0^{out} (as it actually happens for centrally aligned fibers) then the overall propagation in the SMF-MMF-SMF resembles a "quasi-single mode" propagation where the transmitted $\vec{E}_{\mathrm{in}}(t)$ is efficiently transmitted to $\vec{E}_{\mathrm{out}}(t)$ and, most importantly, the modal delays appearing in (1) have much less impact than for MMF IM-DD system, as we show later.

(1) thus allows to model propagation in a SMF-MMF-SMF system, including generic lateral offsets in the SMF-MMF and MMF-SMF transitions, using [12] for the coupling coefficients and [21] for the modal delays. By Fourier transforming (1), we conclude that the transmitted PM-QAM signal undergoes the following $[2 \times 2]$ frequency-dependent transfer function matrix:

$$\boldsymbol{H}(f) = \sum_{m=0}^{M-1} \rho_m^{\mathrm{in}} \boldsymbol{J}_m e^{-j2\pi f \tau_m} \rho_m^{\mathrm{out}} \qquad (2)$$

From a system point of view, the received PM-QAM signal is thus attenuated, due to the fact that the ρ coefficients are all smaller than one, and frequency distorted, due to the resulting dependence on frequency that is evident in (2) and that is physically generated by the differential mode delays on the higher order modes and by the birefringence effects $\boldsymbol{J}_m$.

Finally, it can be shown that the matrix in (2) is in general not unitary (even if the $\boldsymbol{J}_m$ "per mode" Jones matrixes are unitary) and thus an equivalent polarization dependent loss (PDL) is present in SMF-MMF-SMF propagation. Qualitatively, the resulting loss, PDL and spectral dependence increase when increasing lateral offset from an ideal central launching conditions. The quantitative analysis of this effect is one of the key goals of this paper and will be analyzed by simulation and experiments in the next Sections III and IV.

B. SMF-MMF-SMF System With MMF Connectors

While the derivation in the previous section is sufficient for an SMF-MMF-SMF system made of a single MMF fiber without connectors inside it, and it allows to grasp the fundamental issues of SMF-MMF-SMF propagation for PM-QAM signals, it is actually not sufficient for a realistic MMF data center environment, where typically the MMF path is made of different MMF segments due to the presence of patch panels and connectors for an easy reconfiguration of the MMF link. The actual situation we will analyze in this Subsection is the one schematically shown in Fig. 2 with n connectors C_n and $N = n + 1$ MMF segments. The connectors at the MMF-MMF interfaces typically have (small but relevant) lateral alignment offsets [17] so that the coupling coefficients $\rho_{m,k}$ from mode m at the output of

an MMF span and mode k in the following MMF span depend on the lateral offset and must be properly computed. To do so, we can use again the analytical model presented in [12]. We thus developed a numerical propagation simulator taking into account all these effects and moreover assuming that:

1) modes inside different mode groups do not couple
2) modes inside the same mode group strongly and randomly couple but without power loss inside the mode group, an effect that we model as a multi-mode birefringence using random unitary matrices.
3) modal delays can be assumed to be identical for all modes belonging to the same mode group and modeled as described in [21]
4) coupling between modes at the interface between two consecutive MMFs can be evaluated as introduced in [12].

We now focus on expressing the propagation of the modes from the input of one MMF segment to the input of the next one. To this end, we introduce the following vector to represent the $2M$ fields at the input of the nth MMF segment (i.e. two fields on x and y polarization for each of the M MMF modes):

$$
\boldsymbol{E}_n^{MMF}(t) = \begin{bmatrix} E_0^x(t) \\ E_0^y(t) \\ \vdots \\ E_m^x(t) \\ E_m^y(t) \\ \vdots \\ E_{m+N_g}^x(t) \\ E_{m+N_g}^y(t) \\ \vdots \\ E_{M-1}^x(t) \\ E_{M-1}^y(t) \end{bmatrix} \begin{matrix} \text{mode group 1} \\ \\ \cdot \\ \cdot \\ \text{mode group g} \\ \cdot \\ \cdot \\ \cdot \\ \\ \text{mode group } M_g \end{matrix} \quad (3)
$$

where we have highlighted the separation in mode groups with different number of modes through horizontal lines, assuming the presence of M_g mode groups, each containing N_g modes (or actually $2N_g$ after considering birefringence). For instance, the first mode group only contains the fundamental mode and thus $N_1 = 1$.

We can then express, moving to the frequency domain, the matrix transfer function from the MMF segment n to the next MMF segment $n+1$ as follows:

$$
\boldsymbol{E}_{n+1}^{MMF}(f) = \boldsymbol{H}_n^{MMF}(f) \cdot \boldsymbol{E}_n^{MMF}(f) \quad (4)
$$

where (omitting the dependence on frequency f for notation simplicity):

$$
\boldsymbol{H}_n^{MMF} = \boldsymbol{\rho}_{n \to n+1}^{MMF} \cdot \boldsymbol{D}_n^{MMF} \cdot \boldsymbol{J}_n^{MMF} \quad (5)
$$

We now explain the different component of this fundamental equation. The matrix $\boldsymbol{J}_n^{MMF}$ takes into account the birefringence and the mode coupling inside each mode group, and can be expressed as the $[2M \times 2M]$ matrix in Fig. 3: where, for each mode group g, we have indicated the $[2N_g \times 2N_g]$ random unitary submatrices $RU_{2N_g x 2N_g}^g$ generated by the previously described "per mode" birefringence. For an MMF, the first mode group, indicated with index 0, only contains the fundamental

Fig. 3. $[2M \times 2M]$ $\boldsymbol{J}_n^{MMF}$ matrix containing the $[2N_g \times 2N_g]$ random unitary submatrices for each mode group.

mode and gives rise to the RU_{2x2}^0 matrix. The same is true for the second mode group, while for instance two modes belong to the third mode group (index 2). In general, the submatrix for a generic mode group g has dimension $[2N_g \times 2N_g]$, where N_g is the number of modes inside the gth mode group. We point out that the matrix in Fig. 3, even though composed of unitary submatrices on its diagonal, is in general not unitary, an observation that will be useful later on.

The matrix $\boldsymbol{D}_n^{MMF}$ in (5) takes into account the modal delays, so that, in the frequency domain, it has the following diagonal structure:

$$
\boldsymbol{D}_n^{MMF} = \begin{bmatrix} 1 & 0 & 0 & 0 & 0 & 0 & 0 & 0 & \cdots \\ 0 & 1 & 0 & 0 & 0 & 0 & 0 & 0 & \cdots \\ 0 & 0 & e_2^n & 0 & 0 & 0 & 0 & 0 & \cdots \\ 0 & 0 & 0 & e_2^n & 0 & 0 & 0 & 0 & \cdots \\ 0 & 0 & 0 & 0 & e_3^n & 0 & 0 & 0 & \cdots \\ 0 & 0 & 0 & 0 & 0 & e_3^n & 0 & 0 & \cdots \\ 0 & 0 & 0 & 0 & 0 & 0 & e_3^n & 0 & \cdots \\ 0 & 0 & 0 & 0 & 0 & 0 & 0 & e_3^n & \cdots \\ 0 & 0 & 0 & 0 & 0 & 0 & 0 & 0 & \cdots \\ \vdots & \vdots & \vdots & \vdots & \vdots & \vdots & \vdots & \vdots & \ddots \end{bmatrix} \quad (6)
$$

where $e_g^n = e^{-j2\pi f \tau_g^n}$ is the frequency dependent term for each mode group g propagating inside the nth MMF section with a differential delay τ_g^n.

Finally, the last matrix $\boldsymbol{\rho}_{n \to n+1}^{MMF}$ in (5) models the coupling coefficients $\rho_{n \to n+1}^{m,k}$ between the mode m of the nth MMF and the mode k of the following MMF $n+1$ segment (taking also into account lateral offsets in the connectors) and can be expressed as (7) shown at the bottom of next page.

When considering N consecutive MMF segments as in Fig. 1, we can then cascade (5) N times and evaluate the field at the

end of the last MMF segment as:

$$\boldsymbol{E}_N^{MMF} = \boldsymbol{H}_N^{MMF} \cdots \boldsymbol{H}_2^{MMF} \cdot \boldsymbol{H}_1^{MMF} \cdot \boldsymbol{E}_1^{MMF} \qquad (8)$$

Finally, to obtain a global matrix transfer function for our SMF-MMF-SMF system, we still need to take into account the input SMF-MMF coupling and the output MMF-SMF coupling, expressing them as:

$$\boldsymbol{E}_1^{MMF} = \boldsymbol{\rho}_{SMF \to MMF} \cdot \boldsymbol{E}_{IN}^{SMF} \qquad (9)$$

$$\boldsymbol{E}_{OUT}^{SMF} = \boldsymbol{\rho}_{MMF \to SMF} \cdot \boldsymbol{E}_N^{MMF} \qquad (10)$$

In Eqs. (9) and (10), the $\boldsymbol{\rho}_{MMF \to SMF}$ and $\boldsymbol{\rho}_{SMF \to MMF}$ factors represent the $[2 \times 2N]$ matrix of the coupling coefficients of all the modes of the last MMF to the LP$_{01}$ mode of the output SMF, and the $[2N \times 2]$ matrix of the coupling coefficients of the LP$_{01}$ mode of the input SMF to all the modes of the first MMF, respectively. When perfect alignment with no offset is ensured at both the SMF-MMF and MMF-SMF interfaces, as we assume in our analysis, these coupling coefficients are the same at the two transitions and the matrices can be expressed as transposed of each other as in (11).

$$\boldsymbol{\rho}_{MMF \to SMF} = \boldsymbol{\rho}_{SMF \to MMF}^T$$
$$= \begin{bmatrix} \rho_0 & 0 & \rho_1 & 0 & \cdots & \rho_{M-1} & 0 \\ 0 & \rho_0 & 0 & \rho_1 & \cdots & 0 & \rho_{M-1} \end{bmatrix} \qquad (11)$$

In the end, considering the frequency dependent transfer function of the system due to the modal delays, the input to output relation of the Coh-MMF scheme can be obtained combining Eqs. (8), (9) and (10), leading to the following expression:

$$\begin{bmatrix} E^x(f) \\ E^y(f) \end{bmatrix}_{OUT} = \boldsymbol{H}_{TOT}(f) \cdot \begin{bmatrix} E^x(f) \\ E^y(f) \end{bmatrix}_{IN} \qquad (12)$$

where $\boldsymbol{H}_{TOT}(f)$ is the overall $[2 \times 2]$ matrix frequency response of the SMF-MMF-SMF systems, and in particular it is the transfer function seen by the coherent transceiver which leads to distortions in the received PM-QAM signal. To numerically address the resulting system penalty, we developed a Matlab

simulator that can generate these matrices, discretizing the frequency axis over N_f values, so that $\boldsymbol{H}_{TOT}(f)$ actually contains a 3D matrix with $[2 \times \times 2N_f]$ elements.

Taking advantage of a large dataset of fiber modal delays, which includes 16489 OM3 and 3772 OM4 fibers characterized for several values of lateral offsets from 0 μm to 25 μm, we can analytically model a wide variety of Coh-MMF system configurations, varying also the number N of MMF-MMF connectors. The dataset was presented in [21] for SWDM wavelengths down to 850 nm and then transformed for coherent wavelengths around 1550 nm through the theoretical functions developed in [23], using the Sellmeier parameters of the fiber core and cladding to estimate the changes in mode groups with wavelength.

Once the transfer function of the specific fiber link is computed through the frequency-resolved equations presented in this Section we want to estimate the system sensitivity penalty in dB for a given PM-QAM optically un-amplified transmission system [7]. To avoid CPU-time consuming time domain simulation, we developed a fast and reliable tool for coherent transmission performance estimation that works on any possible end-to-end matrix transfer function $\boldsymbol{H}_{TOT}(f)$ in presence of additive Gaussian noise at the receiver. It assumes linearity in MMF field transmission (which is always true in the case of interest for this paper) and the typical digital signal processing (DSP) of any coherent receiver, including clock, polarization and carrier phase recovery, plus adaptive equalization at the end of the chain. Further details and validation of this model can be found in [24].

III. MONTE-CARLO SIMULATIVE ANALYSIS OF COHERENT TRANSMISSION OVER OM3 AND OM4 FIBERS WITH CONNECTORS OFFSETS

The goal of this Section is to numerically evaluate the system power penalty due to the SMF-MMF-SMF link under different conditions. To this end, we use the simulation tool described in previous Section II to perform an extensive analysis of dual-polarization 25 GBaud PM-16QAM (200 Gbit/s raw bit rate) coherent transmission over a generic SMF-MMF-SMF

$$\boldsymbol{\rho}_{n \to n+1}^{MMF} = \begin{bmatrix} \rho_{n \to n+1}^{0,0} & 0 & \rho_{n \to n+1}^{0,1} & 0 & \cdots & \rho_{n \to n+1}^{0,M-1} & 0 \\ 0 & \rho_{n \to n+1}^{0,0} & 0 & \rho_{n \to n+1}^{0,1} & \cdots & 0 & \rho_{n \to n+1}^{0,M-1} \\ \rho_{1,0} & 0 & \rho_{n \to n+1}^{1,1} & 0 & \cdots & \rho_{n \to n+1}^{1,M-1} & 0 \\ 0 & \rho_{n \to n+1}^{1,0} & 0 & \rho_{n \to n+1}^{1,1} & \cdots & 0 & \rho_{n \to n+1}^{1,M-1} \\ \vdots & \vdots & \vdots & \vdots & \cdots & \vdots & \vdots \\ \rho_{n \to n+1}^{M-1,0} & 0 & \rho_{n \to n+1}^{M-1,1} & 0 & \cdots & \rho_{n \to n+1}^{M-1,M-1} & 0 \\ 0 & \rho_{n \to n+1}^{M-1,0} & 0 & \rho_{n \to n+1}^{M-1,1} & \cdots & 0 & \rho_{n \to n+1}^{M-1,M-1} \end{bmatrix} \qquad (7)$$

optical path. Monte-Carlo numerical simulations are run on 300 OM3- or OM4-based configurations, each one affected by 30 different randomly generated realizations of the Jones matrix for each mode, distributed uniformly according to the Haar measure. Moreover, a variable number N of equally spaced MMF connectors ranging from 0 to 4 is considered, so that all the resulting MMF sections have the same length. Thus, for a given number of connectors in the MMF optical path we have 9000 possible transfer functions of the optical channel. The 300 configurations are obtained by randomly selecting the fibers from the aforementioned fiber dataset and by randomly varying the connector radial offset according to a Rayleigh distribution with mean up to 3 μm, which is shown in [19] to be a realistic assumption for installed MMF connectors. Moreover, we investigated Rayleigh distribution mean down to 1 μm to account for technological advancements that might have improved connectors quality in the recent years. In contrast, we assumed that the offset at the SMF-to-MMF and MMF-to-SMF transitions, respectively at the transmitter and receiver side, is considered equal to zero to ensure perfect central launch conditions, as it would be reasonable for a coherent transceiver engineered for Coh-MMF solutions.

For a given transmitted power and receiver noise, each of the 9000 cases results in an SNR value at the equalizer output that we compare against the SNR that we would get in a back-to-back (BtB) configuration without MMF in the system. The key metric is the system penalty in dB on the SNR (due to the SMF-MMF-SMF propagation effect) which, as shown in [7] is directly related to the resulting power penalty in dB. Thus, in the following, we will show the ΔSNR parameter, defined as the difference between the SNR required by the Coh-MMF system to have a $BER = 10^{-2}$ and the SNR required in BtB at the same target BER. This target BER level, although higher than what is usually considered acceptable for short reach communications systems (in the order of $5 \cdot 10^{-5}$ for power consumption limitations), has been chosen to compare analytical results with experimental results obtained by using a commercial coherent card equipped with a soft-decision FEC (see Section IV). Moreover, the experiments show an increasing BER floor with the connector offset due to the stronger effect of modal dispersion, and a proper comparison at low BER would have been unfeasible (see Section IV and [25]).

We point out that two PM-QAM polarizations have (randomly) different performance depending on the specific realization of the Jones matrices, since the matrix $\boldsymbol{H}_{TOT}(f)$ described in previous Section II is not unitary. Although system performance is driven by an intermediate SNR value, we consider the worst case scenario and will show the highest of the two resulting "per polarization" ΔSNR. In order to quantify this polarization dependence, we will later present one graph showing the statistics of the resulting polarization dependent loss (PDL), calculated as difference (in dB) between the power P_{RX}^x and P_{RX}^y of the x and y PM-QAM received signals.

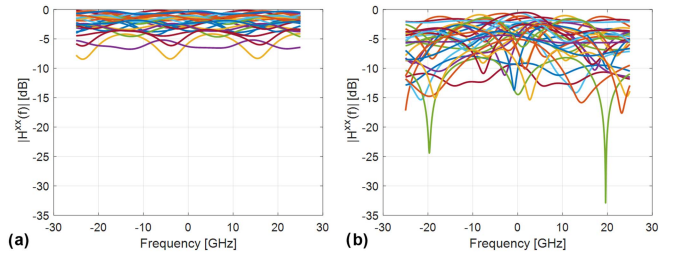$$PDL_{\text{dB}} = P_{RX}^x|_{\text{dBm}} - P_{RX}^y|_{\text{dBm}} \qquad (13)$$

Fig. 4. 30 realizations of the $H^{xx}(f)$ transfer function for one of the 300 configurations of a 25 GBaud 220 m OM3-based Coh-MMF system with a) no MMF connectors or b) 4 MMF connectors.

where:

$$P_{RX}^x = \int (|H^{xx}(f)|^2 + |H^{xy}(f)|^2) \cdot \mathcal{G}_{TX}(f)\, df \qquad (14)$$

and:

$$P_{RX}^y = \int (|H^{yx}(f)|^2 + |H^{yy}(f)|'') \cdot \mathcal{G}_{TX}(f)\, df \qquad (15)$$

where $H^{xx}(f)$, $H^{xy}(f)$, $H^{yx}(f)$ and $H^{yy}(f)$ are the four components of the $[2 \times 2]$ $\boldsymbol{H}_{TOT}(f)$ transfer function matrix and $\mathcal{G}_{TX}(f)$ is the power spectral density of the transmitted signal on each of the two PM components, which we assume in the following to be a square root raised cosine (SRRC) spectrum with 0.2 roll-off factor.

To understand the results coming from our numerical simulator, we start by showing in Fig. 4 30 realizations of the $H^{xx}(f)$ transfer function for one of the 300 configurations when no MMF connectors (Fig. 4(a)) or 4 MMF connectors (Fig. 4(b)) are included in a 25 GBaud 220 m OM3-based Coh-MMF system. The offset distribution in the 4-connector case has a 3 μm mean value. The frequency response of the system does not have the usual low-pass profile, but rather a randomly frequency-dependent evolution. Moreover, Fig. 4(b) highlights a large variation of the amplitude of the transfer function, with frequency dips stretching down to −30 dB. On the other hand in the ideal case with no connectors, the frequency response is much flatter and the total amplitude excursion among the 30 cases is limited to about 8 dB. From this first numerical results it is evident that, apart from the random fluctuations, the transfer function are much more distorted and attenuated when the lateral offsets are present, leading to an increase in system penalty expressed through the ΔSNR metric.

In Fig. 5 we plot the results of a very large Monte-Carlo simulation of the 25 GBaud 220 m OM3-based Coh-MMF system, that we summarize showing the inverse cumulative distribution function (ICDF) of the ΔSNR parameter for number of connectors from 0 to 4 and for two values of the offset Rayleigh distribution mean, 1 μm (solid) and 3 μm (dashed). This graph leads to the first important system level conclusions in this paper, since it gives the statistical probability of a given level of system power penalty introduced by the distortion on $\boldsymbol{H}_{TOT}(f)$ for two different average offset per connector and for different number of connectors (from 0 to 4) in the MMF link. As expected, an increasing number of connectors affects the total
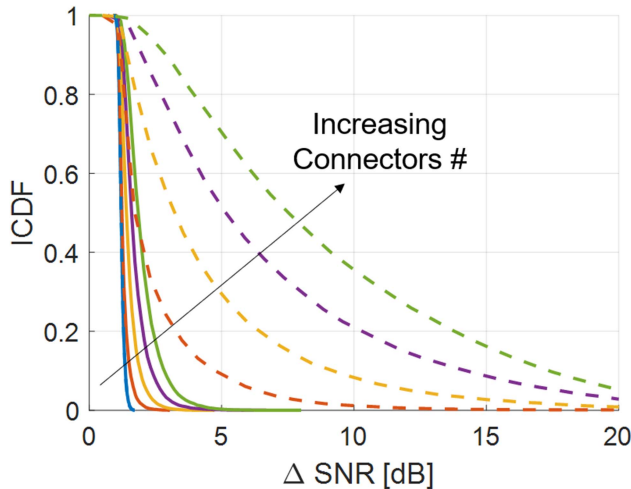
Fig. 5.   ICDF of the ΔSNR parameter for number of connectors from 0 (blue curve) to 4 (green curve) and for offset Rayleigh distribution mean of 1 μm (solid) and 3 μm (dashed).
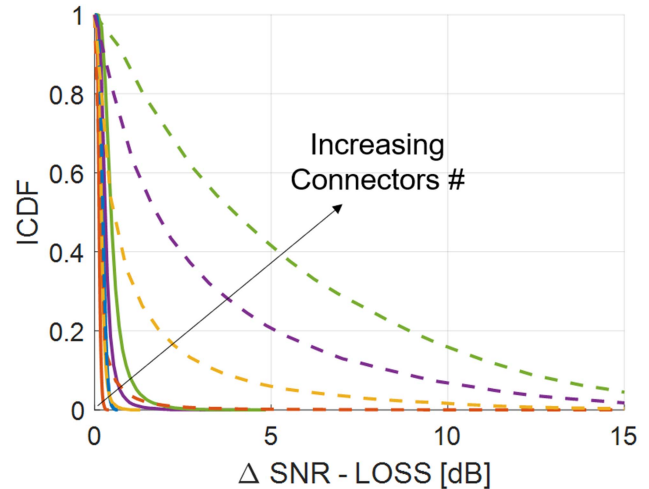

Fig. 6.   ICDF of the $\Delta SNR - Loss$ parameter in a 25 GBaud 220 m OM3-based Coh-MMF system for number of connectors from 0 to 4 and for offset Rayleigh distribution mean of 1 μm (solid) and 3 μm (dashed).

TABLE I
ΔSNR IN dB FOR 99% OF THE 9000 CASES

Connectors	Mean = 1 μm	Mean = 2 μm	Mean = 3 μm
0	1.2	1.2	1.2
1	2.1	8.5	10.5
2	2.8	11	19.4
3	3.6	13.4	23.6
4	4.3	15.2	26

TABLE II
$\Delta SNR - Loss$ IN dB FOR 99% OF THE 9000 CASES

Connectors	Mean = 1 μm	Mean = 2 μm	Mean = 3 μm
0	0.2	0.2	0.2
1	0.5	0.6	2.2
2	0.6	2.2	11.4
3	1.2	5.7	16.7
4	2	10.6	19.2

SNR penalty of the system to an extent that greatly depends on the offset distribution mean. For a low value of 1 μm mean, the ΔSNR is below 4.5 dB even when four connectors are present on the MMF path. When a high, but still possible, 3 μm mean value is considered, the tails of the ICDFs can reach much higher SNR penalty.

Table I summarizes the system performance analysis in terms of SNR penalty, showing the value of the ΔSNR parameter for 99% cumulative probability (i.e. the level at which the ICDF is equal to 0.01), for three mean values for the offset (1, 2 and 3 μm) and for different numbers of MMF connectors. The ICDF curves for a 2 μm offset mean are not shown in Fig. 5 for clarity. When the offset distribution mean is low (i.e. 1 μm), the SNR degradation is very low, even for 4 connectors along the link. This is the first fundamental result of the paper, that shows that for offset with mean value of 1 μm the proposed system can actually work very well, as it will also be confirmed experimentally in the next Section. For higher offsets mean of 2 and 3 μm, the penalty then increases significantly with the number of connectors.

We investigated on the nature of this SNR penalty ΔSNR and we saw that it is the result of two different contributions: the end-to-end optical power net loss due to the connectors being laterally displaced (i.e. the power loss that can be measured by a power meter between the two SMF pigtails), and the SNR degradation related to the transfer function specific features in frequency. To better investigate this last point, Fig. 6 shows the latter, i.e. the difference between the ΔSNR and the net loss

calculated as the ratio between the total transmitted power to the total received power on the input and output SMF pigtails. We wanted to show this specific contribution to the system penalty since it represents the penalty generated by the receiver equalizer to compensate for the frequency un-flatness of the $\boldsymbol{H}_{TOT}(f)$ channel. Comparing Fig. 6 with the previous Fig. 5, it is evident that this "equalizer-induced" penalty is significantly lower than the ΔSNR penalty or, from another point of view, that a significant part of the ΔSNR penalty is simply due to a net power loss in the SMF-MMF-SMF system.

Table II shows this equalizer-induced SNR penalty, for variable numbers of connectors and Rayleigh mean in the 25 GBaud 220 m OM3-based system. For 99% of the cases, the Coh-MMF SNR penalty is always below 2 dB when the offset distribution mean is 1 μm, regardless of the number of MMF connectors. However, it grows to about 19 dB in the worst simulated case of 4 connectors with a 3 μm Rayleigh mean.

We now focus on giving an indication of the polarization dependent penalty, i.e. the fact that the ΔSNR shows two (randomly) different values on the two PM-QAM components. To quantify this effect for variable number of connectors and Rayleigh mean values in a 25 GBaud 220 m OM3-based Coh-MMF system, we show in Fig. 7 the ICDF of the PDL (defined as in (13)), focusing on the range of interest around 0.01, that is the 99% of the simulated Coh-MMF cases. When the offset distribution mean is low (1 μm, solid curves) the performance on the two polarizations is comparable for up to 2 connectors, with less than 0.8 dB difference, whereas it is about 2dB for 4
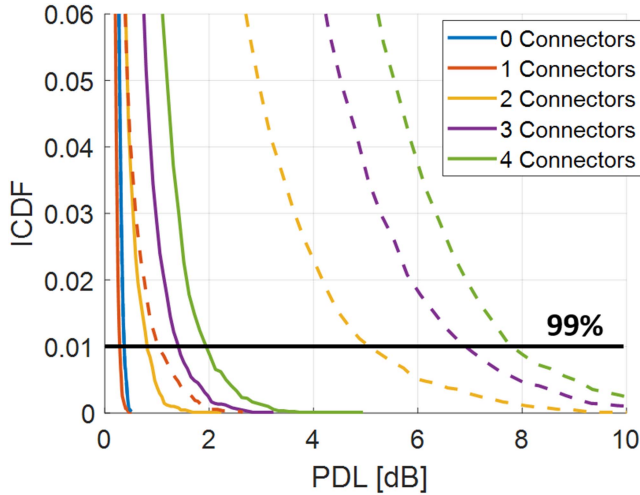
Fig. 7. ICDF of the PDL in a 25 GBaud 220 m OM3-based Coh-MMF system for number of connectors from 0 to 4 and for offset Rayleigh distribution mean of 1 μm (solid) and 3 μm (dashed).

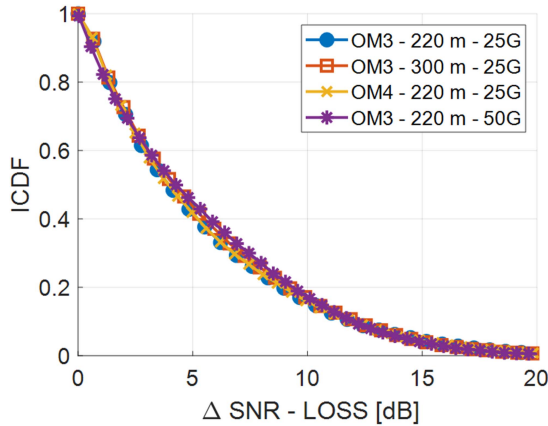Fig. 8. ICDF of the $\Delta SNR - Loss$ parameter for 4 connectors and 3 μm offset Rayleigh distribution mean for a 25 GBaud 220 m OM3 link (blue, dot), 25 GBaud 300 m OM3 link (red, square), 25 GBaud 220 m OM4 link (orange, cross), 50 GBaud 220 m OM3 link (purple, asterisk).

connectors. For a 3 μm mean (dashed curves) the effect of the connectors increases drastically, and the PDL increases up to 8 dB for 4 MMF connectors.

The results depicted in Figs. 5, 6 and 7 in terms of ΔSNR, $\Delta SNR - Loss$ and PDL have also been obtained for OM4 fibers and for an overall link length of 300 m, showing negligible difference on a statistical basis. For comparison, Fig. 8 shows the ICDF of the $\Delta SNR - Loss$ parameter for the worst case of 4 connectors with 3 μm offset mean, for 220 m and 300 m OM3-based and for 220 m OM4-based links. This consistency of the results regardless of the fiber length and type can be explained by the previously described quasi-single mode type of operation that creates a sort of mode-filtering effect of the SMF at the receiver input, which effectively reduces the modal delays impact on the system.

For a more complete analysis, the 25 GBaud PM-16QAM configurations have also been simulated at a higher baudrate. Fig. 8 includes the results for the 50 GBaud (i.e. 400 Gbit/s raw
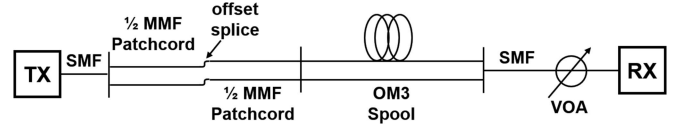

Fig. 9. Experimental setup of the 200 G PM-16QAM Coh-MMF transmission system. MMF: Multimode Fiber; SMF: Single Mode Fiber; VOA: Variable Optical Attenuator.
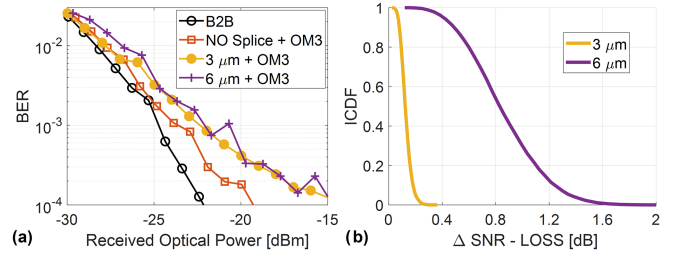

Fig. 10. Measured BER vs received optical power for different configurations of the 200 G PM-16QAM system: back-to-back (black, circle), MMF patchcord with no offset and 296 m OM3 fiber (red, square), 3 μm offset and OM3 fiber (orange, dot), 6 μm offset and OM3 fiber (purple, plus sign). Inset: ICDF of the $\Delta SNR - Loss$ in dB for the 9000 considered cases for 3 μm (orange) and 6 μm (purple) fixed lateral offset.

bit rate) at 220 m OM3-based case with 4 connectors and 3 μm offset mean, showing negligible difference with the 25 GBaud cases in terms of ΔSNR penalty. All the other 50 GBaud configurations with varying number of connectors, length, fiber type and Rayleigh mean value also show no significant penalty with respect to the 25 GBaud counterparts.

IV. EXPERIMENTAL RESULTS

Our experimental setup emulates the configuration presented in Fig. 2 with $N = 2$ sections of MMF and is depicted in Fig. 9. We used a coherent transceiver inside a commercial line card to transmit 200 Gbps net bitrate using PM-16QAM.

Both the transmitter and the receiver are coupled to a short segment of standard SMF. In between, the fiber path is composed of the cascade of a 3 m OM3 MMF patchcord with a 50 μm core diameter and a 296 m long OM3 fiber spool. To study the effect of a misplaced MMF connector, two halves of the MMF patchcord have been fusion spliced together with the wanted lateral offset. The connection of the second half of the patchcord to the input of the OM3 fiber spool, as well as the transitions from SMF to MMF at the transmitter and from MMF to SMF at the receiver, are implemented through lab-grade mating sleeves to ensure central launch conditions without any additional offset on the optical path.

Fig. 10(a) shows the sensitivity curves of the 200 G PM-16QAM Coh-MMF system affected by a variable lateral offset at the fiber facet, compared to the back-to-back configuration with no MMF on the optical path. The results have been obtained through a real-time DSP. The effect of the long OM3 fiber when there is no lateral offset in the MMF patchcord (red curve) is negligible and the penalty with respect to the BtB condition is about 0.4 dB at $BER = 10^{-2}$. The sensitivity penalty increases slightly as the lateral offset is increased to 3 μm and 6 μm,

i.e. moving the center of the facet of the second half of the MMF patchcord from the center along the bisector of the first quadrant of the other facet. A 3 μm offset splice (orange curve) introduces a small penalty of about 0.5 dB. The sensitivity at $BER = 10^{-2}$ then decreases by 1.4 dB when the offset is 6 μm. Fig. 10(b) shows that these experimentally observed values are in good agreement with simulations. The ICDFs of 9000 cases simulated with fixed lateral offset of 3 μm and 6 μm show that SNR penalties can reach up to 0.25 dB and 1.6 dB, respectively, at 99%.

In a 300 m short reach MMF-based system the attenuation on the useful signal would be about 0.3 dB due to the MMF fiber propagation (attenuation below 1 dB/km) and about 6.8 dB due to the connectors offset (from the comparison of Table I and II in the worst case of 4 connectors with a Rayleigh distribution with mean 3 μm). Given the -27.8 dBm sensitivity at $BER = 10^{-2}$ shown in Fig. 10 for a 300 m 200 G PM-16QAM system without offset and assuming a 0 dBm transmitted optical power, we would have about 28 dB of power budget to accommodate the total SNR penalty made of the net optical loss and the equalization penalty due to the frequency dependence of the system transfer function.

A second experimental campaign was performed using a typical off-line approach to be able to extract frequency-domain information from the equalizer. The transmitter is made of an ECL that generates a continuous wave signal at 1550 nm modulated by a Lithium-Niobate dual arm and dual polarization Mach-Zehnder external optical modulator (EOM) operating in single-drive push-pull mode driven by a 64 GS/s arbitrary waveform generator (AWG) working as a four output digital-to-analog converter (DAC) to generate PM-QPSK at 32 GBaud. The input digital stream is a pseudorandom binary sequence (PRBS) of degree 15. The coherent receiver is a commercial FIM24706 by Fujitsu with 22 GHz -3 dB bandwidth. The four electrical signals at the receiver output are acquired through a real time oscilloscope serving as an analog-to-digital converter (ADC) running at 100 GSamples/s and post-processed after proper downsampling at two samples per symbol through an off-line DSP routine in Matlab. The DSP at the transmitter and receiver side is implemented off-line, and includes typically used routines such as a Viterbi&Viterbi algorithm for carrier phase recovery [26] and an adaptive equalizer with 2×2 butterfly-structured FIR filters [27]. The received optical power is varied through a variable optical attenuator (VOA) at the receiver input.

The increasing effect of the fiber birefringence with the lateral offset is confirmed by looking at the normalized Fourier transform of the adaptive equalizer taps w. The equalizer simultaneously compensates electrical bandwidth limitations, polarization rotations and frequency-dependent MMF transfer function when relevant. Inside the signal bandwidth, up to approximately half the baudrate, the equalizer approximately behaves as the inverse of the full system transfer function. Fig. 11 shows one of the four components (the W^{xx} on the diagonal) of the butterfly FIR structure for different values of the received optical power, i.e. on the different points of the sensitivity curves. In Fig. 11(a) the nominal offset is 0 μm, thus the effect of the offset is negligible, the frequency dependence is small and the equalizer mainly performs a mild high-pass filtering to compensate for
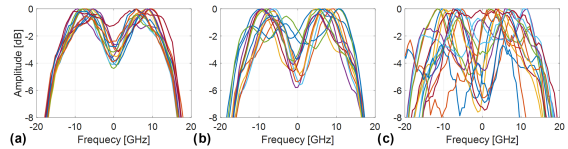

Fig. 11. Normalized Fourier transform of the adaptive equalizer taps (component W^{xx}) for different values of the received optical power when the offset splice is a) 0 μm, b) 3 μm and c) 6 μm.

the optoelectronic bandwidth limitations (nearly symmetrical transfer function). As the offset increases to 3 μm and 6 μm (Fig. 11(b) and (c), respectively) the MMF fiber delays become relevant and an increasing amount of power is transferred into higher order modes. As a result the frequency dependence becomes stronger and an asymmetric behavior between positive and negative frequencies can be observed, showing that this effect is not related to electrical components, but rather to the overall transfer function of the system being modified by the scrambled propagation of the modes inside the MMF, due to the presence of a lateral offset.

V. DISCUSSION AND CONCLUSION

Coherent technology will likely be the next leap in ultra-high speed short-reach links such as intra-datacenter interconnects. In this optical communication segment MMF-based plants are still widespread and their reuse can contribute to an overall reduction of the cost of a technology switch. We have presented a statistical and experimental analysis of the coherent transmission performance over an SMF-MMF-SMF system. Assuming that the coherent transceiver specific for this application would be SMF-coupled and that central launch condition would be ensured at the interface between the SMF at the transmitter and the first section of MMF, we have focused our attention on the impact of lateral offset at the transition from one MMF to another along the optical path, for instance at the points where patch panels are located inside the datacenter. To study modes propagation we have implemented an analytical tool that calculates the modes coupling coefficients at the interface between two fibers, and then developed a model that computes the resulting transfer function of the SMF-MMF-SMF system taking into account the effect of fiber birefringence on the modes, individually.

By using a large database of fiber modal delays and by randomly varying the birefringence per mode, we have analytically generated 9000 transfer functions for each system configuration, including a variable number of MMF-to-MMF connections and considering various link lengths, fiber types and baudrates. We have then developed an analytical model to obtain the SNR at the output of an adaptive equalizer, for each of the generated system frequency responses, without the need for lengthy time domain simulations based on the split-step Fourier method and bit error counting. The results have been obtained considering a polarization multiplexed 25 GBaud transmission based on 16QAM modulation. The statistical analysis of the results shows that, with respect to the BtB configuration, the Coh-MMF system penalty (the SNR penalty net of the optical power loss) at $BER = 10^{-2}$ for 99% of the simulated cases is negligible when the MMF connectors have a low offset distribution mean of 1 μm.

In this case up to 4 connectors can be tolerated with a penalty below 2 dB. Poor quality connections, modeled through a high 3 μm offset distribution mean, result in a system penalty as high as 19.2 dB when 4 connectors are present on the MMF path. We have also experimentally characterized a Coh-MMF system based on 296 m OM3 fiber, by offset splicing two pieces of MMF. The sensitivity results show an increasing penalty of about 0.5 dB and 1.4 dB for 3 μm and 6 μm offset, respectively. On the other hand, when no offset is introduced, that is when central launch condition is ensured throughout the optical link, the penalty with respect to the BtB is only about 0.2 dB.

To best of our knowledge, for the first time our findings highlight analytically and experimentally the advantages ensured by the coherent solution in the MMF-based intra-datacenter scenario, and quantify the detrimental effect due to a lateral offset introduced by connectors. If we consider 2 dB penalty with respect to the back-to-back transmission, the Coh-MMF system can tolerate 4, 2 or 1 MMF-to-MMF connectors, respectively for 1 μm, 2 μm and 3 μm offset Rayleigh mean distribution.

REFERENCES

[1] J. M. Castro, R. Pimpinella, B. Kose, P. Huang, A. Novick, and B. Lane, "Modal-chromatic dispersion interaction effects for 850 nm VCSEL channels at 100 Gb/s per wavelength," *IEEE/OSA J. Lightw. Technol.*, vol. 39, no. 7, pp. 2067–2076, Apr. 2021.

[2] E. R. Parsons, R. Patterson, J. Young, and P. F. Kolesar, "The impact of effective modal bandwidth on 100G SWDM transmission over 250 m OM5 and left-tilt OM4 multimode fibers," *IEEE/OSA J. Lightw. Technol.*, vol. 36, no. 24, pp. 5841–5848, Dec. 2018.

[3] D. Heckle, T. Irujo, R. Reid, and R. Casteel, "Fiber in the NOW: Trends and new technologies demanding fiber deployment," Presented at BICSI Winter Conf. Exhib. 2020, 2020. [Online]. Available: https://www.bicsi.org/uploadedfiles/PDFs/conference/2020/winter/GS_TUES_2.pdf

[4] J. King, "In support of 200G MMF ethernet PMDs," *IEEE 802.3 Next-Gener. 200 Gb/s 400 Gb/s MMF PHYs Study Group*, Jan. 22, 2018. [Online]. Available: https://www.ieee802.org/3/NGMMF/public/Jan18/young_NGMMF_01a_jan18.pdf

[5] G. Rizzelli *et al.*, "Experimental demonstration of coherent transmission over MMF and of the impact of connectors offset," in *Proc. 22nd Int. Conf. Transparent Opt. Netw.*, 2020, pp. 1–4.

[6] G. Rizzelli, F. Forghieri, and R. Gaudino, "Experimental demonstration of real-time 400G coherent transmission over 300m OM3 MMF," in *Proc. Opt. Fiber Commun. Conf.*, 2022, pp. 1–3, Paper W1G.2.

[7] G. Rizzelli, A. Nespola, S. Straullu, F. Forghieri, and R. Gaudino, "Scaling laws for unamplified coherent transmission in next-generation short-reach and access networks," *IEEE/OSA J. Lightw. Technol.*, vol. 39, no. 18, pp. 5805–5814, Sep. 2021.

[8] D. Donlagic and B. Culshaw, "Propagation of the fundamental mode in curved graded index multimode fiber and its application in sensor systems," *IEEE/OSA J. Lightw. Technol.*, vol. 18, no. 3, pp. 334–342, Mar. 2000.

[9] Z. Tong, Q. Yang, Y. Ma, and W. Shieh, "21.4 Gb/s coherent optical OFDM transmission over 200 km multimode fiber," in *Proc. Joint Conf. Opto-Electron. Commun. Conf. Australian Conf. Opt. Fibre Technol.*, 2008, pp. 1–2.

[10] Y. Ma, Y. Tang, and W. Shieh, "107 Gb/s transmission over multimode fiber with coherent optical OFDM using center launching technique," in *Proc. 35th Eur. Conf. Opt. Commun.*, 2009, pp. 848–849.

[11] J. D. Downie, J. E. Hurley, D. V. Kuksenkov, C. M. Lynn, A. E. Korolev, and V. N. Nazarov, "Transmission of 112 Gb/s PM-QPSK signals over up to 635 km of multimode optical fiber," in *Proc. 37th Eur. Conf. Exhibit. Opt. Commun.*, 2011, pp. B363–B369.

[12] A. Amphawan, F. Payne, D. O'Brien, and N. Shah, "Derivation of an analytical expression for the power coupling coefficient for offset launch into multimode fiber," *IEEE/OSA J. Lightw. Technol.*, vol. 28, no. 6, pp. 861–869, Mar. 15, 2010, doi: 10.1109/JLT.2009.2034475.

[13] J. M. Castro, R. Pimpinella, B. Kose, and B. Lane, "Investigation of the interaction of modal and chromatic dispersion in VCSEL–MMF channels," *J. Lightw. Technol.*, vol. 30, no. 15, pp. 2532–2541, 2012, doi: 10.1109/JLT.2012.2203351.

[14] F. H. Robert Fischer, "Linear equalization," in *Precoding and Signal Shaping for Digital Transmission*, ch. 2, Sec. 2.2.4. New York, NY, USA: Wiley, 2002, pp. 35–43.

[15] The Optical Internetworking Forum, "Flex coherent DWDM transmission framework document," 2017. [Online]. Available: https://www.oiforum.com/wp-content/uploads/2019/01/OIF-FD-FLEXCOH-DWDM-01.0-1.pdf

[16] X. Zhou, R. Urata, and H. Liu, "Beyond 1 Tb/s intra-data center interconnect technology: IM-DD OR coherent?," *J. Lightw. Technol.*, vol. 38, no. 2, pp. 475–484, Jan. 2020.

[17] P. Pepeljugoski *et al.*, "Development of system specification for laser-optimized 50μm multimode fiber for multigigabit short-wavelength LANs," *IEEE/OSA J. Lightw. Technol.*, vol. 21, no. 5, 1256–1275, May 2003.

[18] J. King, "Connector loss budgeting methodology for parallel multimode PMDs," in *Proc. IEEE P802.3ba 40 Gb/s 100 Gb/s Ethernet Task Force Interim Meeting*, May 15, 2008. [Online]. Available: https://www.ieee802.org/3/ba/public/may08/king_01_0508.pdf

[19] A. Brunsting and R. Pimpinella, "Lateral offsets for multimode fiber (MMF) connectors part 1," Panduit Corp., Tinley Park, IL, USA, Dec. 13, 2004. [Online]. Available: https://slidetodoc.com/lateral-offsets-for-multimode-fiber-mmf-connectors-part/

[20] P. Pepeljugoski, S. E. Golowich, A. J. Ritger, P. Kolesar, and A. Risteski, "Modeling and simulation of next-generation multimode fiber links," *IEEE/OSA J. Lightw. Technol.*, vol. 21, no. 5, pp. 1242–1255, May 2003, doi: 10.1109/JLT.2003.811320.

[21] P. Torres-Ferrera *et al.*, "Statistical analysis of 100 Gbps per wavelength SWDM VCSEL-MMF data center links on a large set of OM3 and OM4 fibers," *IEEE/OSA J. Lightw. Technol.*, vol. 40, no. 4, pp. 1018–1026, Feb. 2022. doi: 10.1109/JLT.2021.3129455.

[22] W. Xiong *et al.*, "Complete polarization control in multimode fibers with polarization and mode coupling," *Light Sci. Appl.*, vol. 7, no. 1, pp. 1–10, 2018.

[23] J. M. Castro, R. J. Pimpinella, B. Kose, Y. Huang, A. Novick, and B. Lane, "Spectral dependence of multimode fiber modal bandwidth," in *Proc. Opt. Fiber Commun. Conf. Expo.*, 2008, pp. 1–3.

[24] G. Rizzelli, P. Torres-Ferrera, and R. Gaudino, "An analytical model for SNR prediction in coherent systems after generic jones matrices," 2022, *arXiv:2202.11692.*

[25] Q. Wang, Y. Yue, X. He, A. Vovan, and J. Anderson, "Accurate model to predict performance of coherent optical transponder for high baud rate and advanced modulation format," *Opt. Exp.*, vol. 26, no. 10, pp. 12970–12984, 2018.

[26] S. J. Savory, "Digital coherent optical receivers: Algorithms and subsystems," *J. Sel. Topics Quantum Electron.*, vol. 16, no. 5, pp. 1164–1179, Sep./Oct. 2010.

[27] K. Kikuchi, "Fundamentals of coherent optical fiber communications," *IEEE/OSA J. Lightw. Technol.*, vol. 34, no. 1, pp. 157–179, Jan. 2016.